Empirical modeling of stress concentration factors using FEA and artificial neural networks for the fatigue design of tubular KT-joints under combined loading

Mohsin Iqbal (M.I.)[1,*], Saravanan Karuppanan (S.K.)[1], Veeradasan Perumal (V.P.)[1], Mark Ovinis (M.O.)[2] and Hina Nouman (H.N.)[3]

1   Mechanical Engineering Department, Universiti Teknologi PETRONAS, Seri Iskandar 32610, Malaysia; saravanan_karuppanan@utp.edu.my, veeradasan.perumal@utp.edu.my.

2   School of Engineering and The Built Environment, Birmingham City University, Birmingham, UK; mark.ovinis@bcu.ac.uk.

3   Department of Mechanical Engineering, University of Engineering and Technology, Taxila, 47080 Taxila, Pakistan; hinaakram41@hotmail.com.

*   Correspondence: mohsin_22005143@utp.edu.my, engineermohsiniqbal@gmail.com; Tel.: +60-11-6509-8596.

Empirical modeling of stress concentration factors using FEA and artificial neural networks for the fatigue design of tubular KT-joints under combined loading

Abstract

The hot spot stress (HSS) approach for the fatigue design of tubular joints requires that peak HSS be known. Peak HSS in tubular joints is usually determined based on the stress concentration factor (SCF) estimated from empirical models developed through extensive experimental investigations and finite element analysis. While peak HSS usually occurs at a KT-joint's crown and saddle points, its location may change if the tubular joint is subjected to a combination of axial, in-plane bending, or out-of-plane bending loads. This study investigated the peak HSS and its location in a typical KT-joint subjected to the combined loading. Specifically, empirical models to determine the SCF around the brace axis have been developed using extensive finite element analysis and artificial neural networks (ANN) simulations. Less than 3% error was noticed between peak HSS determined through developed models and FEA. Hence, the ANN-based SCF equations and principle of superposition can be used to calculate peak HSS rapidly for fatigue design of tubular joints. This methodology is applicable for developing empirical models for SCF in other tubular joints and boundary conditions.

Keywords: tubular joints, empirical modeling, artificial neural networks, stress concentration factor, hot-spot stress, fatigue design.

List of Abbreviations and symbols

API	American Petroleum Institute	t	The thickness of brace (all braces kept same)
ANN	Artificial neural networks	g	The gap between the central and inclined brace
DoE	Design of Experiment	σ_n	Nominal stress
FE	Finite element	β	d/D
FEA	Finite element analysis	γ	$D/2T$
FEM	Finite element method	τ	t/T
HSE	Health and safety executive, British national regulator for workplace health and safety	α	$2L/D$
		ζ	g/D
HSS	Hot spot stress, the maximum principal stress extrapolated at the weld toe	ip_x	Input to ANN
		hn_x	Output of a hidden layer
IPB	In-plane bending moment	W_x	Weight of a neuron
SPSS	Statistical Package for the Social Sciences	B_x	Bias of a layer
SCF	Stress concentration factor	$i_{n,max}$	The upper range of normalized input data
OPB	Out-of-plane bending moment	$i_{n,min}$	The lower range of normalized input data
Peak HSS	Maximum value of hot-spot stress (HSS) around the brace axis	i_{max}	Maximum of dimensionless input data
		i_{min}	Minimum of dimensionless input data
θ	Angle of the inclined brace with chord axis	$o_{n,max}$	The upper range of normalized output data
D	Diameter of chord	$o_{n,min}$	The lower range of normalized output data
d	Diameter of brace (all braces kept same)	o_{max}	Maximum SCF input used for ANN training
T	Thickness of chord	o_{min}	Minimum SCF input used for ANN training

1   Introduction

Jacket-type structures are widely used for offshore infrastructures, with circular hollow sectioned members used owing to their high strength-to-weight ratio, direction-independent stiffness, and low drag. These structures are subjected to fatigue due to environmental loads such as wind, waves, currents, and operation loads due to drilling, production, storage, materials handling, and living quarters. The fatigue design of a jacket involves the fatigue analysis of all its structural components. The fatigue response of tubular joints greatly influences the fatigue life of jackets. A tubular joint is the joining point of two or more circular hollow sectioned (CHS) members. Joints are the most critical part of a jacket.

Three approaches are generally employed for fatigue analysis of tubular joints: experimental, fracture mechanics (FM)-based, and S-N curves-based.[1,2] Experimental investigations are usually costly and time-consuming. It is a standard procedure to use limited experimentation to validate numerical models and use the numerical model for further investigations. The FM-based approach incorporates crack propagation and is mainly used for existing structures when a crack is present in an existing joint. The S-N curve-based method is more straightforward and usually used during the design stage. In this method, maximum stress at the interface of the joining members, called hot-spot stress (HSS), is used to approximate the fatigue life of a tubular joint using an S-N curve. It is the location where a fatigue crack is likely to initiate.[3] The S-N curve incorporates the weld and fabrication-related factors, while geometry and loading conditions are included in the analyzed joint. The HSS is calculated using nominal stress and stress concentration factor (SCF). SCF is a complex function of joint geometry and load direction. There are no analytical equations for estimating SCF in tubular joints. SCF is usually calculated using experimental investigations and detailed finite element analysis (FEA). Various researchers have used results from extensive experimental studies and FEA to formulate empirical models to determine SCF quickly.[4-9]

A KT-joint is frequently used in jackets, as shown in Fig. 1. The fatigue design of a KT-joint involves the estimation of SCF followed by the calculation of the HSS for life estimation using the S-N curve. In practical scenarios, a typical KT-joint will be subjected to various loads. These loads are axial, in-plane bending (IPB), and out-of-plane bending (OPB). It is widely accepted that the maximum HSS occurs at the crown point when KT-joint is subjected to IPB. Similarly, maximum HSS occurs at the saddle point when the KT-joint is under axial or OPB.[10] Empirical equations for the estimation of SCF in KT-joint can be traced back to Potvin[4], Wordsworth[6], Efthimios[7], and Lloyd's register[8]. Efthimios equations were widely accepted in

the offshore industry and included in the American Petroleum Institute (API) guidelines' 17th and onward editions. All these equations give the SCF at the crown or saddle position for different load types. Commonly the SCF is determined at four points: two crowns and two saddles points, and the maximum SCF is used for fatigue life estimation.[11] However, the location of peak HSS due to combined loads may occur somewhere other than the crown/saddle point, depending on the direction and relative magnitudes of the load.[11] The crown and saddle points are illustrated in Fig. 1.
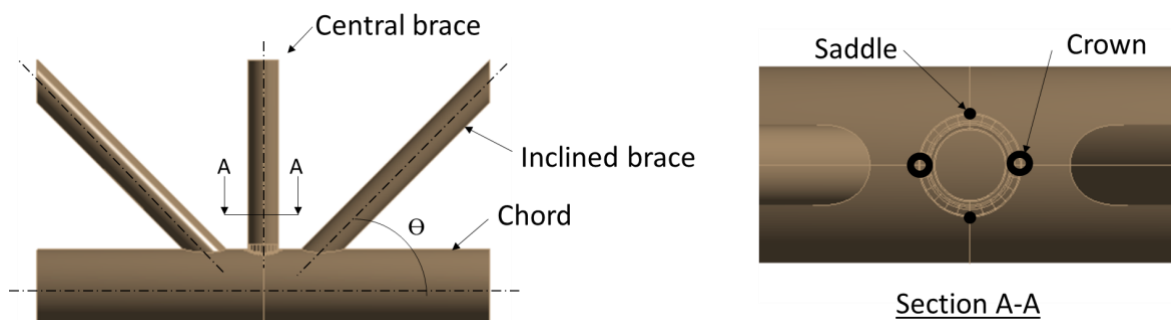
Fig. 1 A typical KT-joint.

Focusing solely on the crown and saddle locations during a fatigue life evaluation can lead to an inaccurate estimation of SCF and fatigue life. Gulati et al.[11] recommended evaluating fatigue life at eight equal-distant points along the interface. However, SCF equations for eight points are not available. The American Petroleum Institute (API) code recommends the principle of superposition to determine the combined HSS peak.[12] Hence, there is a need for empirical models which can be used to determine the SCF around a weld toe. The principle of superposition can then be applied at all points along the weld toe, and the maximum of these, the peak HSS, be used for fatigue life estimation of tubular joints.

Some investigations have focused on the SCF determination along the weld toe. Ahmadi et al.[13], for the first time, presented an empirical model for SCF along the weld toe in a uniplanar double KT-joint subjected to axial load. Lotfollahi-Yaghin et al.[14] examined the inclined brace of KT-joint under the axial load and modeled SCF around the weld toe. Ahmadi et al.[15] studied KT-joint with ring stiffeners under axial compressive load and presented a mathematical model for SCF around the axis of the central brace. The literature covering SCF all around the brace axis is summarized in Table 1. However, only a single load is covered in these studies. Moreover, the SCFs are not accurate, and some further treatment was recommended for the SCF determined through these empirical models. Lotfollahi-Yaghin et al.[14] suggested a multiplication factor of 1.27 for the SCF determined using a mathematical model. Ahmadi et

al.[15] recommended a correction factor of 1.32 for the SCF calculated using this their presented empirical model.

Table 1 Literature coving SCF modeling along the weld toe

Literature source	Joint type	Load type	Tool used for modeling	Further treatment of SCF determined using the Empirical Equation
Ahmadi et al.[13]	Uni-planer DKT-joints	Axial load	SPSS	n/a
Lotfollahi-Yaghin et al.[14]	Uni-planer KT-joint	Axial load	SPSS	Multiplication by a factor of 1.27
Ahmadi et al.[15]	Internal ring-stiffened KT-joint	Axial load	SPSS	Multiplication by a factor of 1.32

To summarize, while combined loading conditions shift the location of the highest SCF away from the crown/saddle points, this has not been incorporated into the fatigue design of jackets and other tubular structures. Some studies have highlighted this issue, but the capability of tools used for empirical modeling resulted in inefficient empirical models.[14–16] New tools must be considered to establish a better correlation between the input variables and the SCF. A promising tool is artificial neural network (ANN), a machine learning tool that can efficiently correlate the input and output of complex systems.[17] Its use has been rapidly increasing in all disciplines, including offshore structure design. Vijaya Kumar et al.[18] revealed the capabilities of ANN integrated with the FEM to approximate complex phenomenon effectively. Miao et al.[19] efficiently modeled the ultimate strength of composite reinforced tubular columns using ANN. The SCF along the weld toe can be approximated with ANN, where other statistical tools have been found unsatisfactory. For example, Dabiri et al.[20] investigated T-joints under tensile and bending loads and developed an ANN to estimate SCF. It was reported that the ANN model outperformed the other models. However, the ANN model was used for SCF determination at a single point. Moreover, ANN was used as a black box, and no further model or empirical equation was derived to estimate SCF. None of the KT-joint investigations has employed ANN for the mathematical modeling of SCF, all the mathematical models were extracted through statistical analysis. In this work, ANN's potential for estimating SCF around the weld toe in complex joints under combined loading was investigated.

This paper presents empirical models for SCF estimation in a KT-joint subjected to combined load. Finite element simulations have been performed using ANSYS, and the generated data is used to train an ANN with SCF as output. Weights and biases of the best epoch are used to develop an empirical model to determine SCF quickly. As the fatigue life of a KT-joint is

generally governed by the peak SCF, and the magnitude of the SCFs at the outer braces is relatively low, only the central brace has been considered in this study.[21]

2 Methodology

Various design configurations of KT-joint were simulated using FEA, and the results were used to train an ANN. Empirical model for HSS estimation around the brace axis were developed for loads in orthogonal directions (axial, IPB, and OPB). The principle of superposition was then used to determine the peak HSS for KT-joint subjected to combined load. All results were validated with FEA. The methodology for this study is shown in Fig. 2. The process of empirical model development starts with the range of parameters defining the joint. These parameters are continuous variables, and hence infinite design configurations can be selected. To limit the design iterations, a specific number of design configurations covering the full range of variables have been selected. This design set has been simulated, and results were used for modeling and training ANN. These steps are described in detail in sections 2.1-2.5.
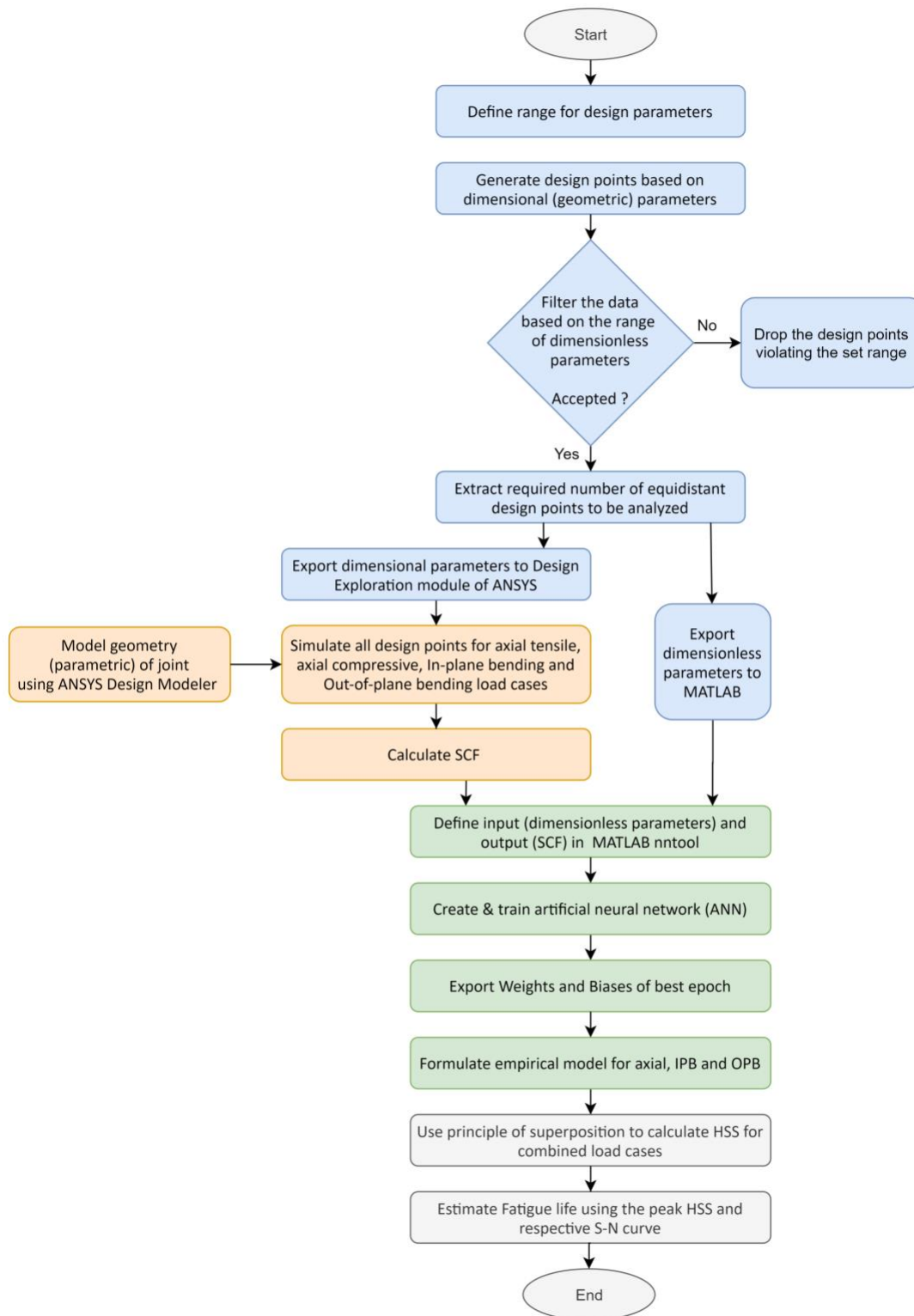
Fig. 2 Methodology for ANN-based modeling of SCF.

2.1 Range of design variables

The design of a typical KT-joint was expressed as a function of dimensionless parameters to obtain a generic empirical expression. Dimensionless parameters are commonly used to

standardize the intended response of a system. The selection of dimensionless parameters for KT-joint was based on literature and the capability of these parameters to represent a wide range of design configurations.[22] These parameters are presented in Equations (1)-(5). The first step was the finalization of the range for design parameters. A typical uniplanar KT-joint comprises one chord and three braces. The load is usually transferred from the brace elements to the chord, and the chord transfers the load to the foundation through the piles. The chord usually has a larger diameter and thickness than the brace. Very large and small-diameter CHS elements are unusual for structural applications in jackets. CHS elements are generally fabricated through the cold rolling of sheets. Substantial thicknesses can induce severe residual stress, which is not acceptable. Minimal pipe thickness may require tight tolerances and can cause welding issues, which is not recommended. Based on these practical considerations, the typical range for CHS joints is used and is shown in Table 2.[9,23–26]

All possible design configurations were generated solely based on dimensional parameters, D, d, T, t, θ, and g, assuming ten possible values for each variable. These 6-sets were used to derive all possible designs ($10^6 = 1000000$). These 10^6 design points had many which violated the range specified for dimensionless design variables. The data was filtered to exclude the out-of-range designs. This cleaned data has had 63900 design points. Simulating all these datasets would have taken too much time. This data was reduced by choosing a pre-set number of equidistance designs and exported to ANSYS for simulation, according to the methodology shown in Fig. 2.

$$\beta = D/d \tag{1}$$

$$\gamma = D/2T \tag{2}$$

$$\tau = t/T \tag{3}$$

$$\alpha = 2L/D \tag{4}$$

$$\zeta = g/D \tag{5}$$

where

D = Chord diameter

d = Brace diameter

T = Thickness of chord wall

t = Thickness of brace wall

L = Length of chord

g = Gap b/w braces at chord surface

Table 2 Range of parameters used for the design of KT-joint.

Type	Parameters	Range	Reference
Dimensionless parameters	β	0.4–0.8	23
	γ	12–20	23
	τ	0.3–0.7	23
	α	5–40	9,24
	ζ	0.25–0.5	15,25,26
Dimensional parameters	Θ	30°–75°	23
	T	3–10 (mm)	Assumed manufacturing limit
	t	3–10 (mm)	Assumed manufacturing limit
	D	200–400 (mm)	Minimum: assumed $(D \geq 150)^9$ Maximum: calculated based on γ_{max} and T_{max}
	d	80–320 (mm)	Minimum: calculated based on β_{max} and D_{min} Maximum: calculated based on β_{max} and D_{max}
	L	1800–3000 (mm)	Minimum: based on α_{max} and D_{max} Maximum: based on α_{min} and D_{min} (Range was further squeezed to limit computational cost)
	g	100 (mm)	26

2.2 Finite element modeling and validation

The initial geometry of KT-joint was modeled according to the dimensions used by Ahmadi et al.[27], as shown in Fig. 3. ANSYS Design Modeler was used for modeling. The dimensional variables in Table 2 were defined as parameters, and the joint geometry was modeled as a function of these variables. Steel was assumed as the joint material with a Modulus of elasticity and Poisson ratio of 207 GPa and 0.3, respectively.[28,29] High-order nonlinear elements were used for meshing the KT-joint. A mesh with 223630 elements was finalized after sensitivity study. A nominal load of 30 MPa was applied on the central brace. The chord ends and inclined brace ends were fixed, and static structural linear elastic analysis was performed. Meshed model and boundary conditions are shown in Fig. 4. The stress response of KT-joint was assessed by measuring the maximum principal stresses at the chord side of the central brace-chord interface. The finite element (FE) model was validated by comparing results to the literature, as shown in Fig. 5.[30] A difference of less than 3% was found between the current results and the simulation results of literature. This FE model was then used for further investigations.
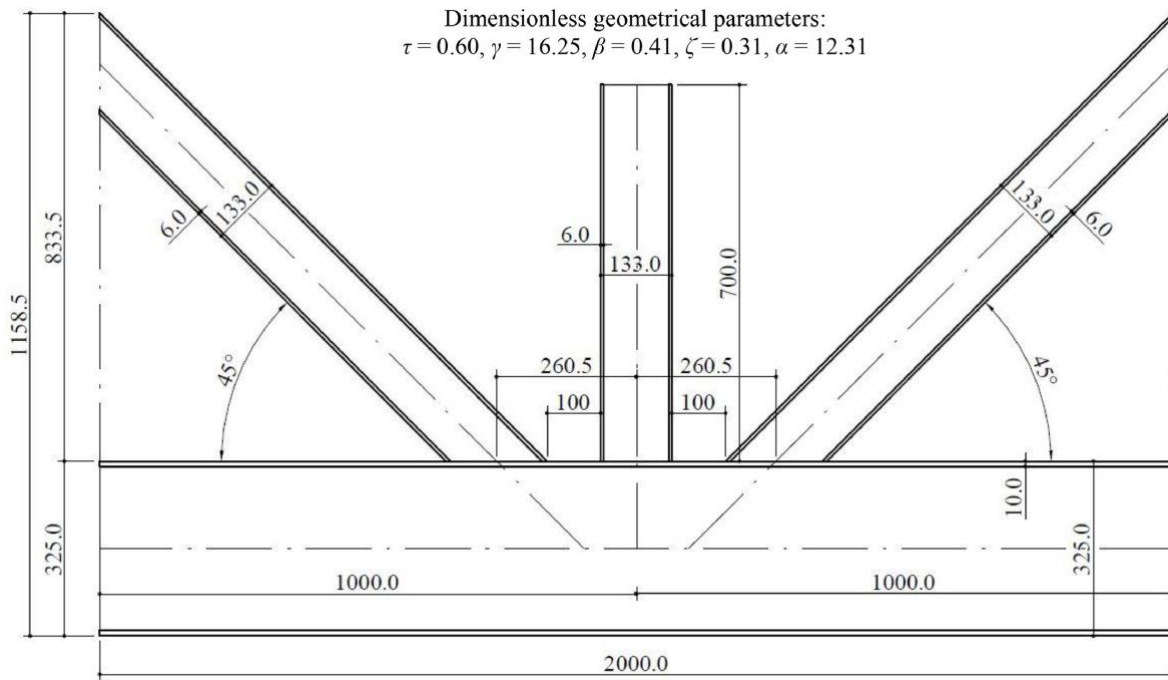
Dimensionless geometrical parameters:
$\tau = 0.60, \gamma = 16.25, \beta = 0.41, \zeta = 0.31, \alpha = 12.31$

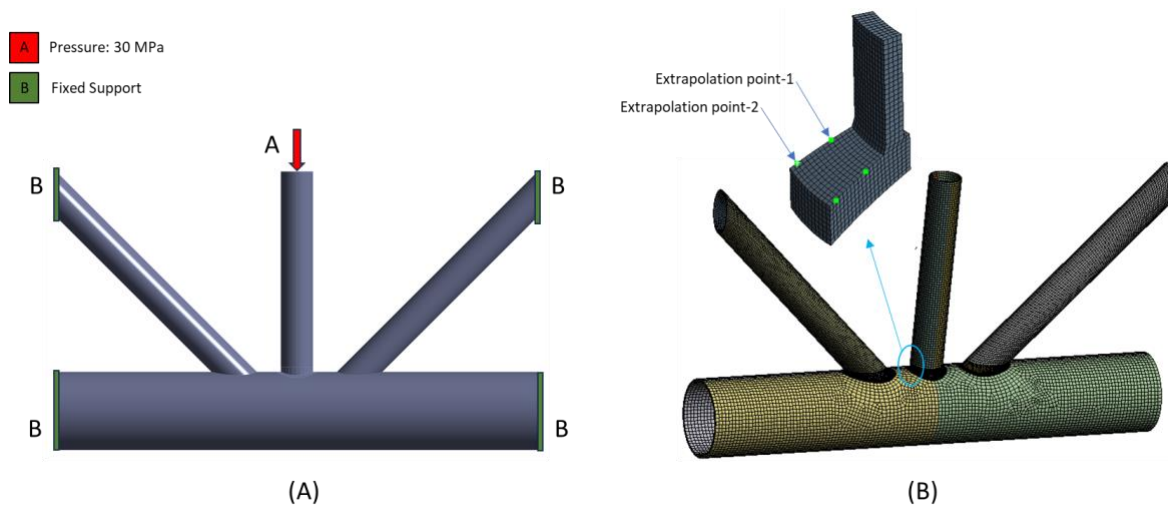Fig. 3 Geometry of KT-joint (unit: mm).[27]

Fig. 4 Model used for simulation. (A) Boundary conditions. (B) Meshed model.

The reference literature used for validation has both simulation and experimental results. There was a 0-15% difference in SCF determined, which was assumed acceptable in that paper.[30] The FE model developed in the current study was coherent with the simulation model of literature; however, a similar difference was noticed from the experimental results of the literature. The magnitude of difference was comparable for both the current work and the simulation results reported in that paper. It can be attributed to some unidentified or undocumented details of the experimental setup, which were ignored by the author of that paper also.[30] The second reason

could be some minor approximations in the dimensions of joints used for experimental investigation, as the SCF depends on the geometric sizing of a joint.
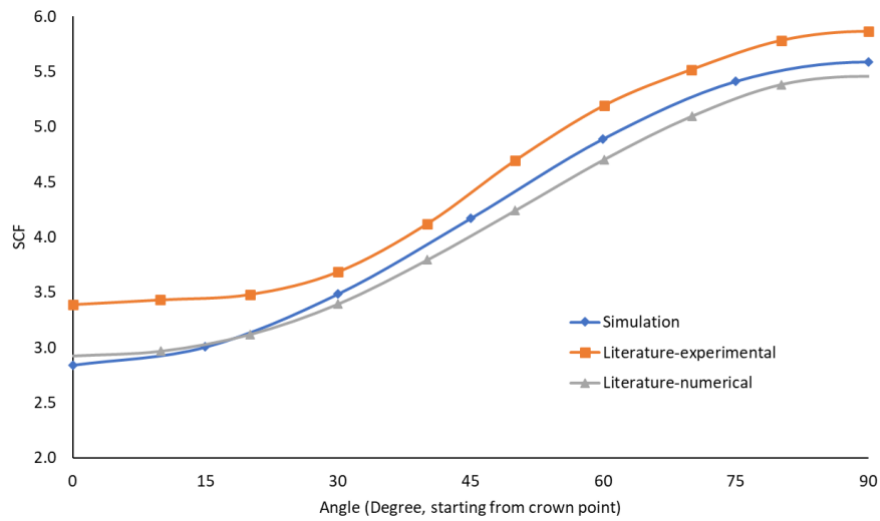

Fig. 5 Validation of the FE model (compressive load on the central brace).

2.3 Simulation of design of experiment

Once the FE model was validated, the design iterations were simulated according to the methodology presented in Fig. 2. It was found that the SCF is independent of sizing (any geometrically scaled version will have the same SCF), load magnitude, and material properties. However, if different geometric parameters are varied differently, the SCF will change. The SCF results remain constant for all geometric sizes qualifying any selected dimensionless design point in the defined range. The structure of KT-joint cannot be uniquely determined with a chosen design point based on dimensionless parameters.

The design dataset was imported to the ANSYS Design Exploration module. All the design sets were simulated, and results were stored for every iteration. A Python script was incorporated to extract stresses at two extrapolation points, at each 15° offset around the axis of the central brace. This way, stress at two extrapolation points was stored for 24 positions in each design iteration. A schematic of stress locations is shown in Fig. 6. These values were used for hot-spot stress calculation.
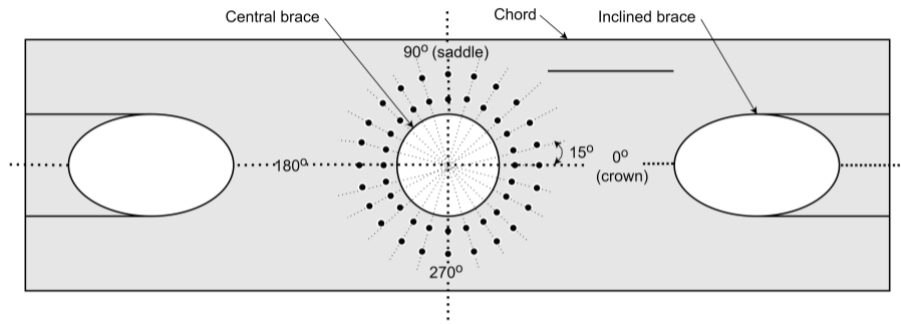
Fig. 6 Extrapolation points around the brace axis.

2.4   Hot-spot stress calculation

Stress at the weld toe exponentially increases due to the geometry of the joint and notch of the weld, as shown in Fig. 7. Numerous physical, metallurgical, thermal, and mechanical aspects of the welding process influence these stress effects.[31,32] In addition, an increase in the number of weld passes results in improved mechanical properties; however, increased residual stresses facilitate the initiation of cracks. It is a well-accepted practice to exclude the effect of weld process and notch geometry while calculating SCF. These effects had already been included in the S-N curve for fatigue life estimation by assuming that the joints used for S-N data extraction had similar.[1] Stresses are measured at some specific distance and then extrapolated at the weld toe. This extrapolated stress is called hot-spot stress (HSS). The HSS of a joint depends on the geometry and loading parameters.
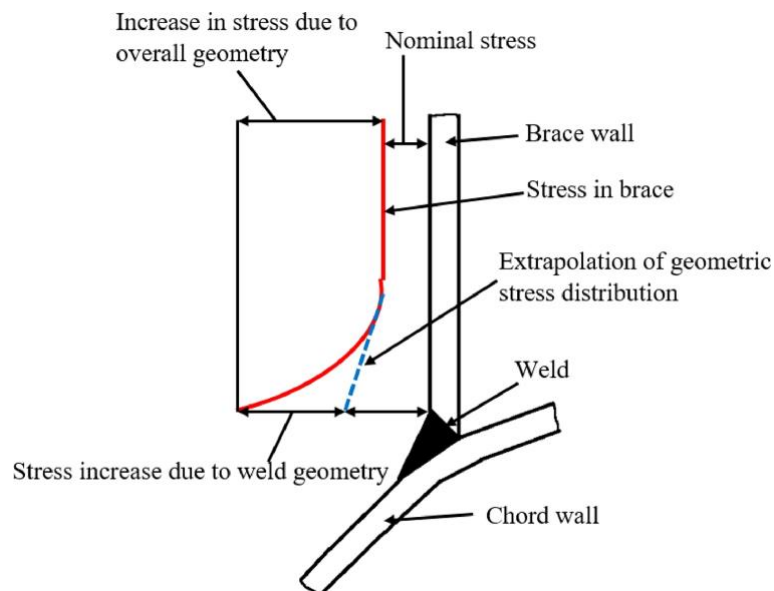

Fig. 7 Stress behavior at tubular joint.[33]

Different types of stress can be used for the hot-spot stress calculation, i.e., principle, directional (normal to weld toe), and von Mises. The type of stress used for calculating hot-spot must be the same as that used for calculating the S-N curve, which will be later used for estimating fatigue life. S-N curves in the literature are usually based on normal or principal stress.[1] The normal and principal stress is approximately equal near the weld toe for simple load cases; however, the von Mises stress differs substantially. A fatigue crack grows along the weld toe, i.e., perpendicular to the normal stress. However, when the principal stress direction differs from that of the normal to the weld toe, fatigue cracking is normal to the principal stress direction.[3] Principal stress at the neighborhood of the chord-brace toe is not orthogonal to the weld toe for combined load cases,[11] indicating that the principal stress is of practical significance for combined load cases. The principal stress gives the truest indication of material failure; however, its calculation during the experimental investigation will require a strain rosette, while the normal stress can be calculated using a unidirectional strain gauge.[1] FE model of this study was validated with the results of Ahmad et al.[30], who had used the maximum principal stress in their investigation; hence the maximum principal stress was used throughout this study. N'Diaye et al.[10] and Bao et al.[34] used von Mises stress for HSS calculation.

The reference point for extrapolation must be near the weld toe but far enough to avoid the influence of the weld notch. Extrapolation points at 0.4T and 1.4T from the weld toe were used, as recommended by the International Institute of Welding.[1] The extrapolation concept is elaborated in Fig. 8. Once hot-spot stress was determined at each 15° along the weld toe, SCF was calculated using Equation (6). The nominal stress can be calculated by dividing the applied load by the cross-sectional area of the brace for axial load and using beam theory for bending loads.[35] Equations (7) and (8) were used to determine the nominal stress.
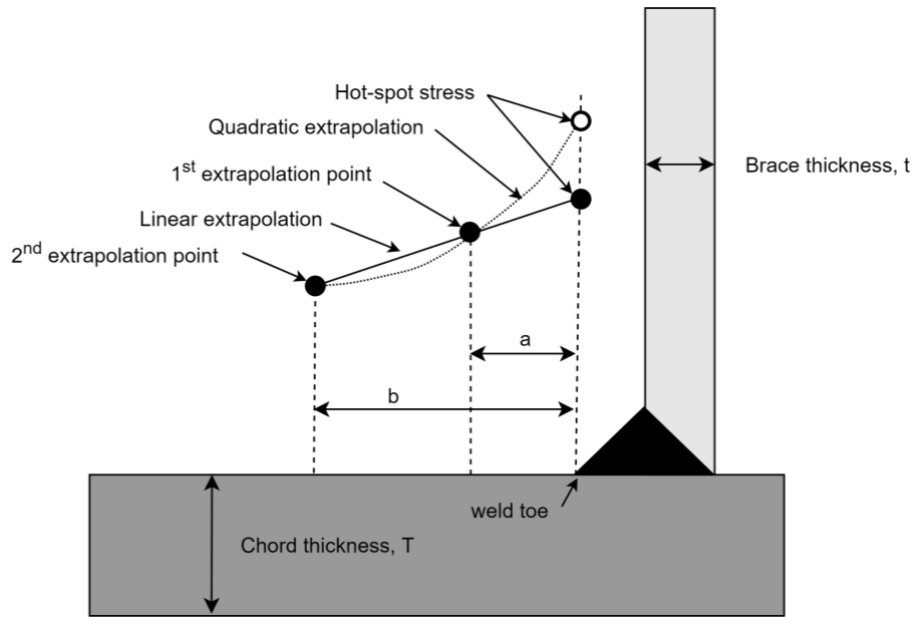
Fig. 8 Linear extrapolation of stress at the weld toe according to IIW.[1]

$$\sigma_{HSS} = SCF * \sigma_n \tag{6}$$

$$\sigma_{n-axial} = \frac{\text{Applied Force}}{\text{cross} - \text{sectional area of the central brace}} \tag{7}$$

$$\sigma_{n-bending} = \frac{32 \, d \, M}{\pi[d^4 - (d - 2t)^4]} \tag{8}$$

where

$\sigma_{HSS} =$	Hot-spot stress (HSS) extrapolated at the weld toe
$\sigma_n =$	Nominal stress
$d =$	Brace diameter
$M =$	Bending moment
$T =$	Thickness of chord wall
$t =$	Thickness of brace wall

2.5 Empirical modeling of SCF using artificial neural networks

Following the methodology presented in Fig. 2, FEA data from ANSYS was exported for modeling ANN. The data imported into MATLAB contained dimensionless parameters as input and SCF as output. This data was loaded into the nntool module of MATLAB, and a neural network was set. Supervised learning formulation was employed using Levenberg–Marquardt backpropagation algorithm.[36] A typical ANN model with three inputs, one hidden layer having two neurons and one output, as shown in Fig. 9. The matrix form of this ANN is represented using Equations (9) and (10). The inputs (ip_x) are connected to each neuron in the adjacent hidden layer (hn_x) through weights (W_x). Every value transferred from the input is multiplied with the corresponding weight, and all are summed up. An activation function $A(x)$ is applied

to the summed product, and the output is added to a bias value $B(x)$. Tansig (tangent sigmoid) and linear transfer functions were used for these layers, given in Equations (11) and (12), respectively. This new sum acts as input to the neuron in the next hidden layer, which continues until the output layer is reached.

The parameters defining the geometry of KT-joints used for modeling and the output SCFs at 24 locations along the weld toe were used for developing ANN. This model was trained using inputs (dimensionless parameters) and outputs (SCF). The coefficient of determination, $R^2 > 0.999$ was deemed acceptable for all training, validation, and testing. Weights and biases for the best epoch were used for empirical modeling. Before using the inputs in empirical expression, they must be normalized for standardization and to prevent the dominance of a variable with larger magnitudes. After calculating with empirical formulas, it is necessary to denormalize the outputs. Expressions for normalization and denormalization are given as Equations (13) and (14).
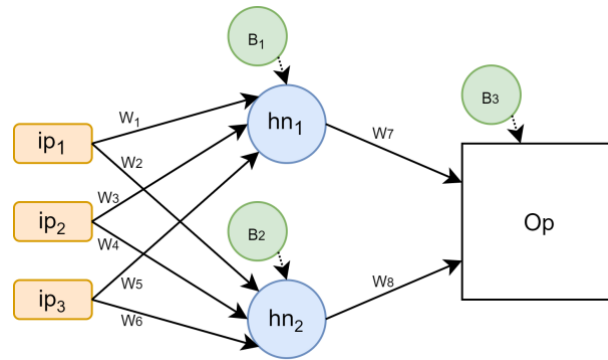

Fig. 9 A typical feedforward neural network.

$$\begin{bmatrix} hn_1 \\ hn_2 \end{bmatrix} = \begin{bmatrix} W_1 & W_3 & W_5 \\ W_2 & W_4 & W_6 \end{bmatrix} \begin{bmatrix} ip_1 \\ ip_2 \\ ip_3 \end{bmatrix} + \begin{bmatrix} B_1 \\ B_2 \end{bmatrix} \tag{9}$$

$$[op] = [W_7 \quad W_8] \begin{bmatrix} hn_1 \\ hn_2 \end{bmatrix} + [B_3] \tag{10}$$

$$A(x) = \frac{2}{1 + e^{-2x}} - 1 \tag{11}$$

$$B(x) = x \tag{12}$$

$$i_{normalized} = \frac{(i_{n,max} - i_{n,min})(i - i_{min})}{(i_{max} - i_{min})} + i_{n,min} \tag{13}$$

$$o_{denormalized} = \frac{(o_n - o_{n,min})(o_{max} - o_{min})}{(o_{n,max} - o_{n,min})} + o_{min} \tag{14}$$

where

ip_x = input to ANN

hn_x = output of a hidden layer

W_x = Weight of a neuron

B_x = bias of a layer

$i_{n,max}$ = 1

i_{max} = max of the original input data

$i_{n,min}$ = -1

i_{min} = min of the original input data

$o_{n,max}$ = 1

o_{max} = max of SCF data used for training

$o_{n,min}$ = -1

o_{min} = min of SCF data used for training

2.6   Principal of superposition

Superposition is a fundamental concept used in physics to combine the effect of linear systems. When two or more systems interact, the resultant is algebraic sum of the individual results. Stress can be superimposed for static loading when the material is linearly elastic. The American Petroleum Institute (API) also permits the superposition of stress.[12] Various expressions have been recommended for determining accumulative HSS.[35,37,38] Combined HSS computed through Equation (15) was found most closer to the FEA and has been used in this study. Results determined through superposition are discussed in the next section.

$$Peak\ HSS = SCF_{ax}\sigma_{nominal\ axial} + SCF_{ipb}\sigma_{nominal\ ipb} + SCF_{opb}\sigma_{nominal\ opb} \qquad (15)$$

3   Results and discussion

A general empirical formulation for calculating hot-spot stress for a central brace of a KT-joint subjected to arbitrary loads was sought. All loads on a joint can be decomposed into axial, IPB, and OPB components. These loads were individually simulated to develop ANN-based empirical models. Various geometric iterations were simulated for each load direction, and the SCF was determined at 24 equidistance locations, 15° apart, starting from the crown position. The generated data was used to model ANN. An ANN with a minimum number of layers and neurons yet offering reasonable accuracy was considered, as shown in Table 3. Empirical models were developed using weights and biases of the best epoch. These empirical models were then revalidated for individual loads using geometric configurations other than those used in ANN. Similarly, the principle of superposition was used to determine HSS under combined load from equations for individual load cases. These results were also validated through detailed FEA. The following sections present the equations and their validation.

Table 3 Summary simulations and ANN training.

Load case	No. of design iteration	No. of hidden layers	No. of neurons	Developed equation	Maximum % error

					$\dfrac{(\text{SCF}_{eq} - \text{SCF}_{FEA})\text{x}100}{\text{SCF}_{FEA}}$
Axial Compression	1901	1	8	(16), (17)	1 %
Axial Tension	937	1	10	(18), (19)	6 %
IPB	929	1	8	(20), (21)	2 %
OPB	929	1	6	(22), (23)	5 %

3.1   Individual axial, IPB, and OPB load

The HSS trend in axial and bending cases is presented in Fig. 10. It is evident that the peak HSS occurs at the saddle point for OPB and axial load; and around the crown position for IPB load. The location of peak HSS for IPB was not exactly the crown point and depended on the joint geometry. A similar observation was reported by Pang et al.[39] The trend of SCF and HSS was symmetric around the orthogonal axis for the loads and boundary conditions considered. Quarter symmetry was found for axial tensile and compressive loads, with half symmetry for IPB and OPB. This half model of IPB and OPB could be further simplified by calculating only 1/4 of the results and then taking the negative (inverted) results for the next quarter model, as these were subjected to either tension or compression of equal magnitude. Hence empirical equations were developed only for a quarter model.

Various combinations of hidden layers and numbers of neurons were investigated. The difference of SCF in a typical KT-joint calculated through ANN to FEA was used as criterion for selecting the optimum ANN configuration. An ANN model with one hidden layer having eight neurons was found to be optimum for compression load in the axial direction. Equations (16) and (17) have been developed for axial compression cases. This model could approximate HSS with less than a 1% error. One hidden layer and ten neurons were optimal for the axial tensile load, with less than 6% error in HSS estimation. Equations (18) and (19) can be used to estimate HSS for KT-joint with a tensile load on the central brace. Equations (20) and (21) were extracted for IPB, while Equations (22) and (23) were for OPB. The maximum error for HSS estimated was less than 2% of IPB and less than 5% for OPB. The accuracy of empirical equations is shown in Fig. 10, compared to the detailed FEA. The peak HSS error was lower, as shown in Table 4.

These empirical equations have been included as MATLAB functions for quick calculation of HSS. The input to these MATLAB functions is dimensionless parameters $(\beta, \gamma, \tau, \theta, \alpha, \zeta)$ defining a typical KT-joint. These parameters have been defined in Equations (1)-(5), with their range shown in Table 2. The attached file will plot HSS for 0°-360° using the results of the

quarter model from the empirical functions. This supplementary data can be provided on request.
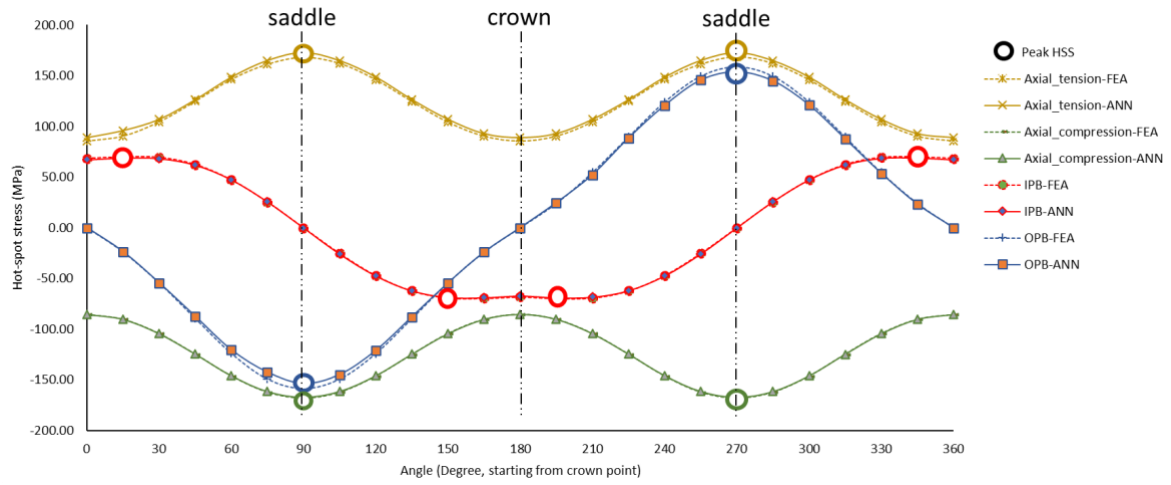

Fig. 10 Hot-spot stress behavior under a single load (30 MPa nominal stress on central brace).

Axial compression:

$$
\begin{bmatrix} h_1 \\ h_2 \\ h_3 \\ h_4 \\ h_5 \\ h_6 \\ h_7 \\ h_8 \end{bmatrix} = \begin{bmatrix} 0.68 & 0.09 & 0.24 & -0.04 & -0.03 & 0.14 \\ -0.06 & 0.13 & -0.06 & -0.07 & -0.07 & 0.00 \\ 0.23 & 0.26 & 0.28 & 0.05 & 0.01 & -0.06 \\ 0.06 & -0.14 & -0.02 & 0.08 & 0.07 & 0.00 \\ 0.04 & -0.07 & 0.14 & 0.03 & 0.06 & 0.00 \\ 0.22 & -0.13 & -0.36 & 0.03 & -0.03 & 0.13 \\ -0.18 & 0.15 & 0.33 & -0.39 & 0.03 & -0.13 \\ 0.00 & -0.10 & -0.26 & -0.25 & -0.08 & 0.04 \end{bmatrix} \begin{bmatrix} \beta_n \\ \gamma_n \\ \tau_n \\ \theta_n \\ \alpha_n \\ \zeta_n \end{bmatrix} + \begin{bmatrix} -1.59 \\ -0.62 \\ -0.98 \\ 0.42 \\ 0.55 \\ 1.58 \\ -1.61 \\ 1.17 \end{bmatrix} \tag{16}
$$

$$
\begin{bmatrix} SCF_0 \\ SCF_{15} \\ SCF_{30} \\ SCF_{45} \\ SCF_{60} \\ SCF_{75} \\ SCF_{90} \end{bmatrix} = \begin{bmatrix} 0.70 & -3.13 & -0.95 & 0.13 & -4.51 & 1.79 & 1.92 & 1.69 \\ 0.56 & -1.39 & -0.58 & 1.59 & -4.18 & 2.08 & 2.02 & 1.91 \\ 0.30 & 4.76 & 0.67 & 6.05 & -2.17 & 1.07 & 0.50 & 2.50 \\ 0.30 & 12.86 & 1.69 & 11.12 & 1.23 & -3.43 & -4.26 & 2.91 \\ 0.45 & 18.07 & 1.73 & 14.03 & 3.73 & -7.75 & -8.55 & 2.87 \\ 0.82 & 20.46 & 1.32 & 15.20 & 5.01 & -10.05 & -10.05 & 2.59 \\ 1.21 & 20.74 & 1.05 & 15.23 & 5.21 & -10.74 & -11.3 & 2.35 \end{bmatrix} \begin{bmatrix} h_1 \\ h_2 \\ h_3 \\ h_4 \\ h_5 \\ h_6 \\ h_7 \\ h_8 \end{bmatrix} + \begin{bmatrix} -0.59 \\ -0.61 \\ -0.32 \\ 0.60 \\ 1.29 \\ 1.88 \\ 2.36 \end{bmatrix} \tag{17}
$$

Axial tensile:

$$
\begin{bmatrix} h_1 \\ h_2 \\ h_3 \\ h_4 \\ h_5 \\ h_6 \\ h_7 \\ h_8 \\ h_9 \\ h_{10} \end{bmatrix} = \begin{bmatrix} 0.32 & -1.27 & 0.80 & -0.55 & -0.47 & -0.50 \\ 0.34 & 0.34 & 0.06 & -0.18 & 0.02 & 0.03 \\ 0.00 & 0.42 & 0.24 & -0.66 & -0.01 & 0.00 \\ -0.78 & 0.69 & -0.28 & -0.33 & 0.19 & -0.19 \\ 0.09 & -0.19 & -0.46 & -0.21 & -0.13 & 0.03 \\ 0.68 & -0.11 & -0.31 & 0.01 & -0.10 & -0.23 \\ -0.10 & -0.27 & -0.55 & -0.41 & 0.15 & 0.10 \\ -0.16 & -0.08 & -0.75 & 0.02 & 0.06 & -0.02 \\ 0.94 & 0.22 & 0.00 & 0.21 & -0.28 & -0.18 \\ -0.13 & -1.37 & 0.21 & 1.38 & -2.10 & 0.86 \end{bmatrix} \begin{bmatrix} \beta_n \\ \gamma_n \\ \tau_n \\ \theta_n \\ \alpha_n \\ \zeta_n \end{bmatrix} + \begin{bmatrix} -1.47 \\ -1.11 \\ -1.17 \\ 0.83 \\ 0.31 \\ 0.35 \\ 1.09 \\ -0.30 \\ 0.60 \\ -0.99 \end{bmatrix} \tag{18}
$$

$$
\begin{bmatrix} SCF_0 \\ SCF_{15} \\ SCF_{30} \\ SCF_{45} \\ SCF_{60} \\ SCF_{75} \\ SCF_{90} \end{bmatrix} =
\begin{bmatrix}
-0.06 & -0.51 & 0.29 & 0.08 & -0.60 & 0.15 & -0.59 & -0.64 & -0.04 & 0.00 \\
-0.04 & -0.47 & 0.36 & 0.10 & -0.64 & 0.05 & -0.46 & -0.65 & -0.01 & 0.02 \\
0.01 & -0.91 & 0.54 & 0.13 & -0.44 & -0.22 & -0.52 & -0.68 & 0.09 & -0.01 \\
0.03 & -1.28 & 0.69 & 0.15 & -0.18 & -0.51 & -0.40 & -0.59 & 0.28 & -0.02 \\
0.01 & -1.34 & 0.81 & 0.17 & -0.06 & -0.58 & -0.40 & -0.53 & 0.37 & -0.02 \\
-0.01 & -1.29 & 0.87 & 0.23 & -0.04 & -0.50 & -0.44 & -0.50 & 0.35 & -0.01 \\
-0.03 & -1.38 & 0.89 & 0.27 & -0.03 & -0.47 & -0.45 & -0.50 & 0.36 & -0.01
\end{bmatrix}
\begin{bmatrix} h_1 \\ h_2 \\ h_3 \\ h_4 \\ h_5 \\ h_6 \\ h_7 \\ h_8 \\ h_9 \\ h_{10} \end{bmatrix} +
\begin{bmatrix} 0.04 \\ 0.09 \\ -0.11 \\ -0.51 \\ -0.57 \\ -0.55 \\ -0.65 \end{bmatrix}
\tag{19}
$$

IPB:

$$
\begin{bmatrix} h_1 \\ h_2 \\ h_3 \\ h_4 \\ h_5 \\ h_6 \\ h_7 \\ h_8 \end{bmatrix} =
\begin{bmatrix}
-0.10 & -0.38 & 0.31 & -0.06 & 0.00 & 0.19 \\
0.07 & -3.13 & -11.51 & -0.32 & 4.84 & 4.99 \\
0.35 & 0.05 & -0.18 & -0.01 & 0.03 & 0.08 \\
0.12 & 0.01 & -0.14 & -0.01 & 0.01 & 0.04 \\
0.45 & 0.00 & 0.23 & 0.11 & -0.07 & -0.18 \\
-0.29 & 0.24 & 0.12 & -0.10 & 0.07 & 0.12 \\
-0.15 & -0.17 & -0.19 & -0.11 & 0.04 & 0.31 \\
1.31 & 0.54 & -0.45 & -0.11 & 0.13 & -0.01
\end{bmatrix}
\begin{bmatrix} \beta_n \\ \gamma_n \\ \tau_n \\ \Theta_n \\ \alpha_n \\ \zeta_n \end{bmatrix} +
\begin{bmatrix} 0.76 \\ 6.95 \\ -0.23 \\ -0.04 \\ 0.39 \\ -0.13 \\ 0.97 \\ 2.15 \end{bmatrix}
\tag{20}
$$

$$
\begin{bmatrix} SCF_0 \\ SCF_{15} \\ SCF_{30} \\ SCF_{45} \\ SCF_{60} \\ SCF_{75} \end{bmatrix} =
\begin{bmatrix}
0.62 & -0.01 & 1.08 & -3.02 & 0.77 & 1.08 & -1.13 & 0.26 \\
0.57 & -0.02 & 0.74 & -2.51 & 0.88 & 1.19 & -0.82 & 0.24 \\
0.67 & -0.01 & -0.15 & -0.71 & 1.10 & 1.40 & -0.85 & 0.24 \\
0.80 & -0.02 & -1.22 & 1.77 & 1.42 & 1.70 & -1.02 & 0.19 \\
0.99 & -0.02 & -2.59 & 5.08 & 1.76 & 2.04 & -1.47 & 0.04 \\
0.13 & -0.02 & -3.41 & 7.26 & 1.94 & 2.27 & -1.83 & -0.09
\end{bmatrix}
\begin{bmatrix} h_1 \\ h_2 \\ h_3 \\ h_4 \\ h_5 \\ h_6 \\ h_7 \\ h_8 \end{bmatrix} +
\begin{bmatrix} 0.14 \\ -0.14 \\ -0.39 \\ -0.55 \\ -0.49 \\ -0.34 \end{bmatrix}
\tag{21}
$$

OPB:

$$
\begin{bmatrix} h_1 \\ h_2 \\ h_3 \\ h_4 \\ h_5 \\ h_6 \end{bmatrix} =
\begin{bmatrix}
0.72 & 0.38 & 0.48 & -1.55 & 0.12 & 0.20 \\
0.54 & -0.15 & 0.16 & 0.00 & -0.01 & -0.01 \\
0.89 & 0.21 & 0.00 & -0.01 & -0.01 & -0.07 \\
0.71 & 0.21 & 0.22 & 0.07 & -0.01 & -0.05 \\
0.27 & 0.25 & -0.32 & 0.03 & -0.01 & 0.00 \\
-0.57 & 0.09 & 0.30 & 0.01 & 0.01 & 0.07
\end{bmatrix}
\begin{bmatrix} \beta_n \\ \gamma_n \\ \tau_n \\ \Theta_n \\ \alpha_n \\ \zeta_n \end{bmatrix} +
\begin{bmatrix} -1.35 \\ -0.66 \\ 0.93 \\ -0.42 \\ -0.63 \\ -0.36 \end{bmatrix}
\tag{22}
$$

$$
\begin{bmatrix} SCF_{15} \\ SCF_{30} \\ SCF_{45} \\ SCF_{60} \\ SCF_{75} \\ SCF_{90} \end{bmatrix} =
\begin{bmatrix}
-0.07 & 2.63 & -0.02 & -2.43 & 2.25 & -0.14 \\
0.01 & 0.84 & -0.64 & -0.98 & 1.28 & -1.35 \\
-0.04 & 0.50 & -1.22 & -0.55 & 1.03 & -1.63 \\
-0.09 & 0.92 & -1.35 & -0.88 & 1.20 & -1.44 \\
-0.11 & 1.40 & -1.31 & -1.20 & 1.36 & -1.18 \\
-0.12 & 1.64 & -1.32 & -1.28 & 1.45 & -1.09
\end{bmatrix}
\begin{bmatrix} h_1 \\ h_2 \\ h_3 \\ h_4 \\ h_5 \\ h_6 \end{bmatrix} +
\begin{bmatrix} 1.94 \\ 0.92 \\ 1.03 \\ 1.33 \\ 1.57 \\ 1.77 \end{bmatrix}
\tag{23}
$$

Table 4 Summary of location and error of peak HSS.

Load case	Load case	Location of peak HSS	% Error at peak HSS
Individual load	Axial Compression	crown	0.30
	Axial Tension	crown	2.30
	IPB	15° from the saddles	1.00
	OPB	saddle	1.90
2 simultaneous loads	IPB + OPB 4:1	45° from the crowns	1.30
	IPB + OPB 2:1	30° from the saddles	0.20
	IPB + OPB 1:1	15° from the saddles	1.00

	IPB + OPB 1:2	15° from the saddles	1.00
	IPB + OPB 1:4	saddle	1.90
	OPB + Axial 4:1	saddle-1	1.60
	OPB + Axial 2:1	saddle-1	1.70
	OPB + Axial 1:1	saddle-1	1.70
	OPB + Axial 1:2	saddle-1	1.90
	OPB + Axial 1:4	saddle-1	1.90
	Axial + IPB 4:1	15° from the saddles	2.30
	Axial + IPB 2:1	15° from the saddles	1.90
	Axial + IPB 1:1	30° from the saddles	1.20
	Axial + IPB 1:2	45° from the saddles	0.10
	Axial + IPB 1:4	30° from the saddles	0.70
3 simultaneous loads	Axial + IPB + OPB 1:1:1	15° from saddle-2	0.56
	Axial + IPB + OPB 1:1:2	saddle-2	0.77
	Axial + IPB + OPB 1:2:1	30° from saddle-2	0.35
	Axial + IPB + OPB 1:2:2	15° from saddle-2	0.79
	Axial + IPB + OPB 2:1:1	15° from saddle-2	0.42
	Axial + IPB + OPB 2:1:2	saddle-2	0.39
	Axial + IPB + OPB 2:2:1	15° degrees from saddle-2	0.41

3.2 Combined load

Once the empirical equations to estimate SCF around the brace axis for axial, IPB, and OPB are available, combined hot-spot stress can be calculated using the principle of superposition.[40] Equation (15) was used for superposition. All possible combinations of the individual loads were simulated. Table 4 presents the peak HSS location for each individual and combined load cases for the KT-joint modeled according to the dimension by Ahmadi et al.[30] A detailed discussion on combined loads is presented in the next section:

3.2.1 Combined IPB-OPB load

The maximum HSS for IPB occurs at 15° from the crown (for the joint considered, as it depends on the joint geometry), while for OPB, it occurs at the saddle point. When IPB and OPB are simultaneously applied on a KT-joint, the location of maximum HSS changes, as shown in Fig. 11. Five cases of combined IPB and OPB were simulated, namely 4:1, 2:1, 1:1, 1:2, and 1:4. The "1" represents a nominal load of 30 MPa. SCFs for the individual load were found using Equations (20)-(23), and then combined HSS was calculated using Equation (15). When a 30 MPa IPB load was applied with 30, 60, and 120 MPa OPB load, the location of the maximum HSS changed to a point between the crown and saddle (45° from the reference saddle point) and 30° and 15° for the latter two cases. For OPB of 30 MPa, with an IPB of 30, 60, and 120 MPa, the HSS peak occurred at 15° for the first two cases and then at the saddle location. This

change in the location of peak HSS highlights the need for empirical models that can determine SCF along the weld toe as well, in addition to the crown/saddle. The developed empirical equations could estimate the location of the peak HSS for combined IPB and OPB. These results were compared to the detailed FEA in which both loads were applied simultaneously. A maximum of 2% error was recorded at the peak HSS points.
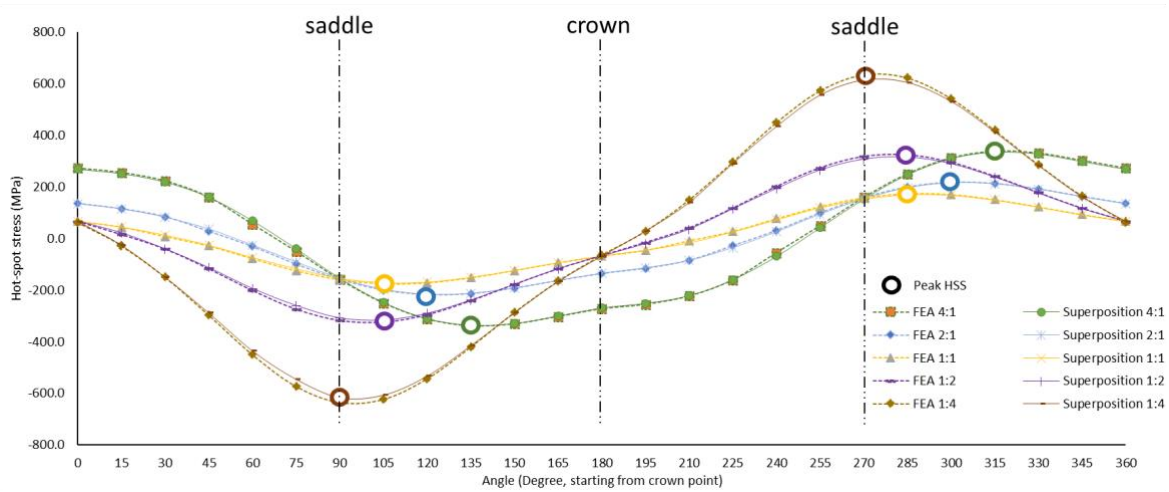

Fig. 11 Hot-spot stress behavior under combined IPB and OPB (nominal stress in multiples of 30 MPa applied on the central brace).

3.2.2 Combined OPB-axial load

Combined OPB and axial loads were simulated for five combinations of nominal loads. The OPB was fixed at 30 MPa, and 30, 60, and 120 MPa axial compression/tension loads were simulated. Similarly, the axial load was fixed at 30 MPa, and 30, 60, and 120 MPa of OPB load was applied. The trends of HSS for these load configurations are shown in Fig. 12 and Fig. 13. Peak HSS for OPB remained at the saddle. The stress was opposite at both saddles—one side is in compression, and the other is in tension. The HSS peak for individual axial load also occurs at the saddle, positive (tension) for tensile load and negative (compression) for compressive load compression. The HSS peak due to OPB occurs at both saddles, one compressive and the other tensile. It was found that the HSS is either tensile or compressive, as the individual loads combine for a global peak at the saddle point. For the OPB-compressive axial case, the peak was found at the saddle at the compressive side of OPB, as shown in Fig. 12. Whereas for the combined OPB-tensile axial, the peak was found at the saddle at the tensile side of OPB, as shown in Fig. 13.
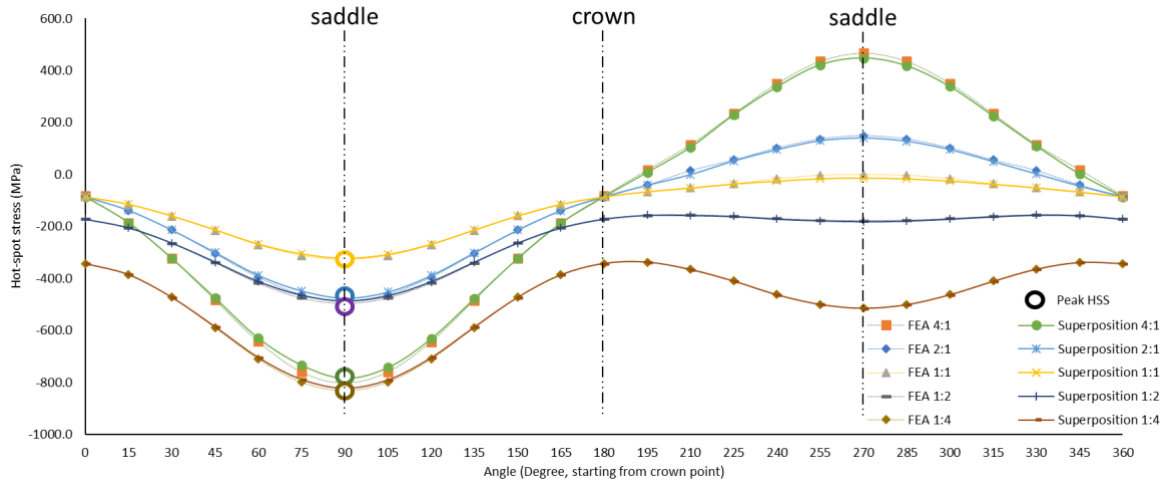
Fig. 12 Hot-spot stress behavior under combined OPB-axial compression (nominal stress in multiples of 30 MPa applied on the central brace).
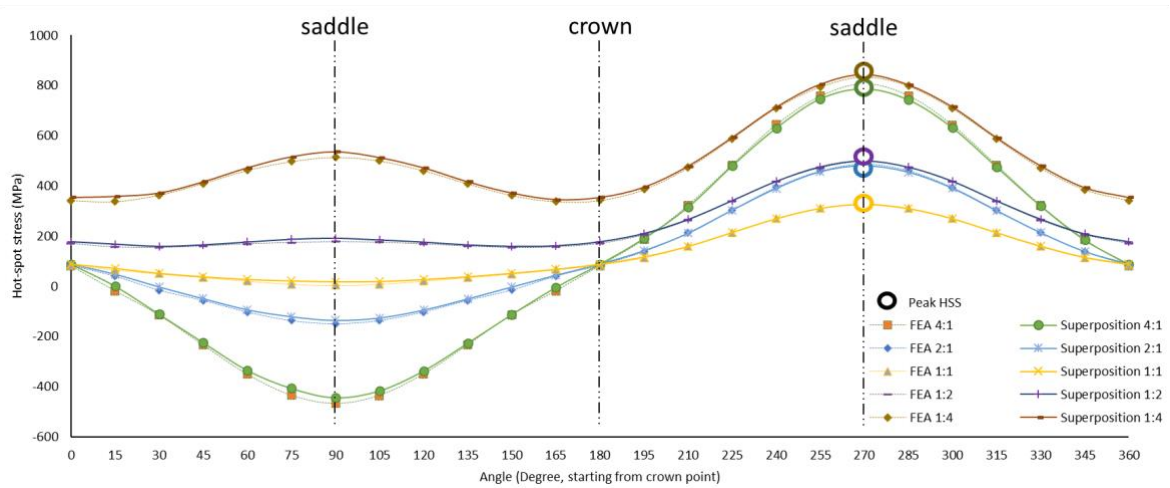

Fig. 13 Hot-spot stress behavior under combined OPB-axial tension (nominal stress in multiples of 30 MPa applied on the central brace).

The ANN-based empirical models for OPB, axial compression, and axial tension were used to estimate HSS for these individual load components, and then combined HSS was determined using superposition. These outputs were validated with HSS calculated through FEA, and the peak HSS error was less than 2%.

3.2.3 Combined IPB-axial load

Simultaneous IPB and axial loads were simulated for five similar load combinations. The location of peak HSS was different for each load case, as shown in Fig. 14 and Fig. 15, depending on the relative magnitude of the load components. The ANN-based equations and

the superposition were used to estimate peak HSS, and this value was compared to the results obtained through detailed FEA. A maximum error of 3% was noticed in peak HSS determined through both methods.
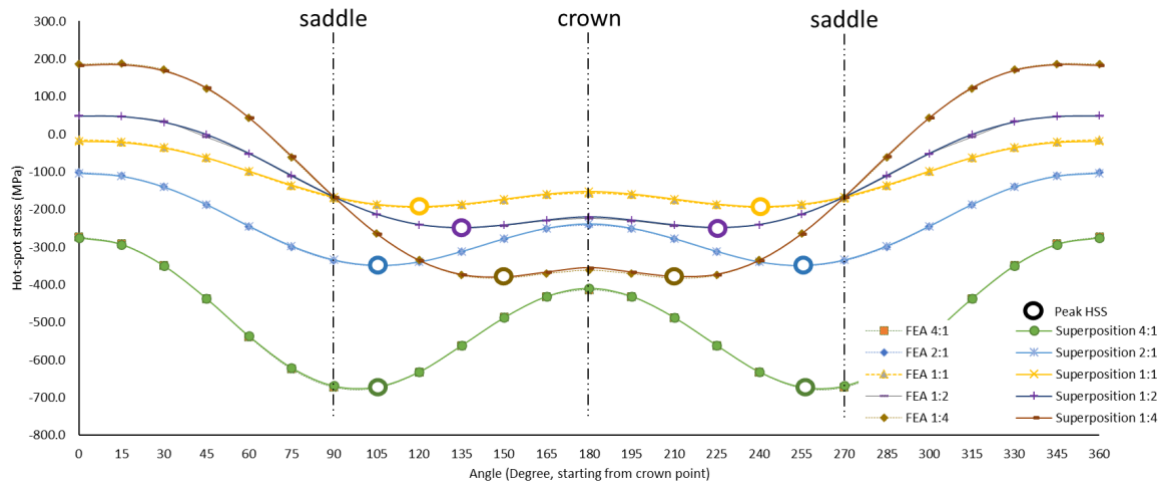

Fig. 14 Hot-spot stress behavior under combined IPB-axial compression (nominal stress in multiples of 30 MPa applied on the central brace).
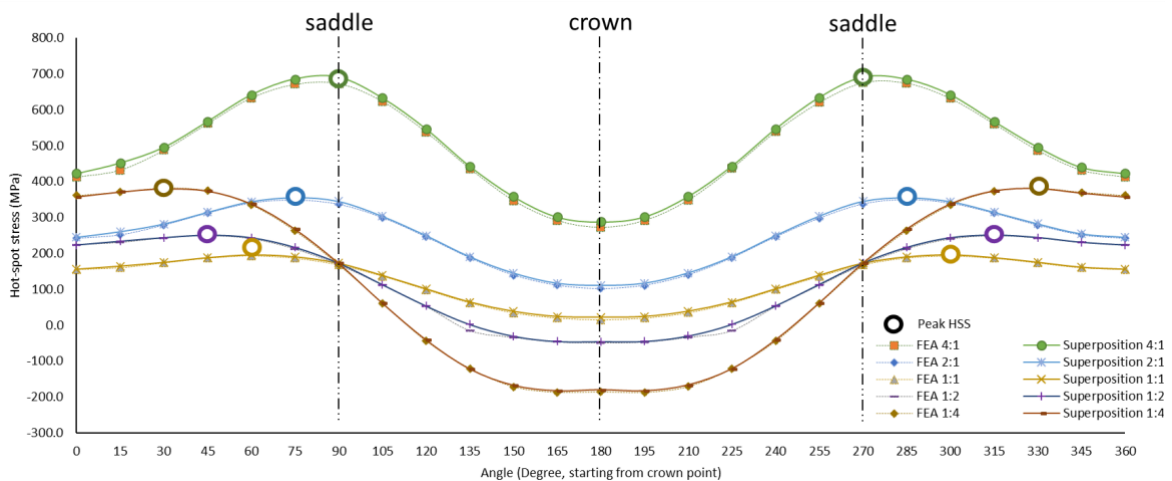

Fig. 15 Hot-spot stress behavior under combined IPB-axial tension (nominal stress in multiples of 30 MPa applied on the central brace).

3.2.4 Combined axial-IPB-OPB load

A typical KT-joint may be simultaneously subjected to axial, IPB, and OPB loads. Only magnitudes of 30 MPa and 60 MPa were considered for nominal stress to limit the number of simulations. Seven different combinations of simultaneous loading were simulated, and the

peak HSS was determined, as shown in Fig. 16. Peak HSS determined through the empirical models with an error of less than 1%. Although there is little scatter in the locations of peak HSS, it could widen depending on the relative magnitudes of load components.
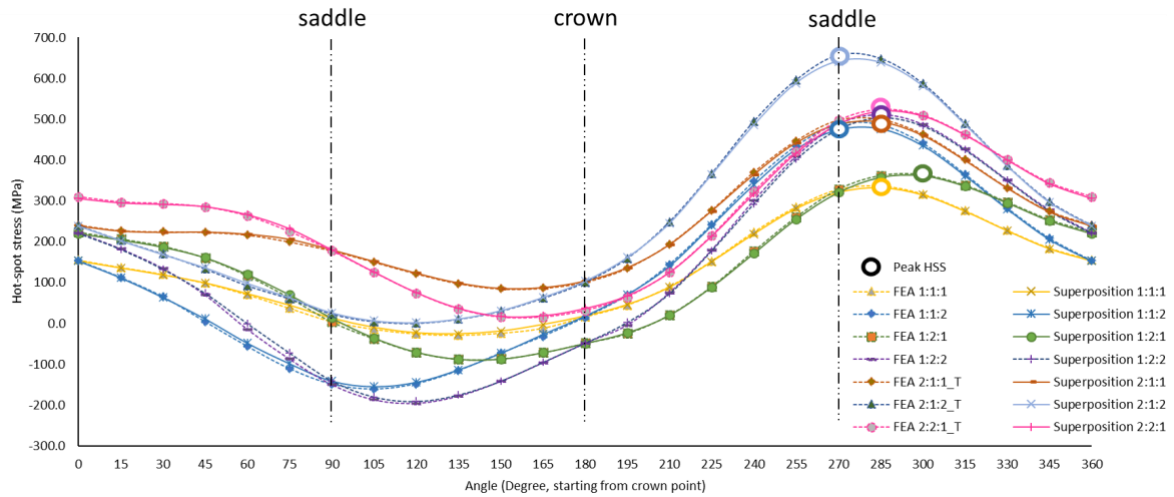

Fig. 16 Hot-spot stress behavior under combined IPB-axial tension (nominal stress in multiples of 30 MPa applied on the central brace).

4   Conclusion

An empirical model to determine the stress concentration factor (SCF) on the central brace of KT-joints for combined loading was developed for fatigue life estimation. Artificial neural networks (ANN)-based mathematical modeling has been successfully employed for predicting peak hop-spot stress (HSS) with the ANN-based empirical equations used to estimate the SCF and superposition used for determining the HSS. The developed equations can estimate peak HSS with less than 3% error. The empirical models can be used for combined axial, in-plane bending, and out-of-plane bending loads. Since these equations are applicable from 0°–360°, the peak HSS under combined load can always be determined and is not limited to the saddle/crown. Hence, using ANN has enabled the quick estimation of SCF and then the hot-spot stress around the brace axis for complex loading. A KT-joint simulation was accomplished in 4-5 minutes using finite element analysis for determining HSS, whereas the same was calculated in a few seconds using the empirical model. Moreover, it has been proved that the existing models for SCF at crown/saddle are insufficient to estimate peak HSS under combined loads. Investigations into the defects, such as cracks or corrosion in joints and their inclusion in the empirical equations, can widen the applicability of the presented methodology. Fatigue analysis of tubular joints with recent methods like strain-based, notch stress, averaged strain

energy density, stored plastic strain energy density, and linear elastic fracture mechanics approach; and experimental validation would be helpful for comparations.

Data availability

Supplementary data is available upon request.

Author contributions

Conceptualization, S.K. and M.I.; Methodology, M.I.; Analysis, M.I. and H.N.; Validation, M.I.; Writing Original Draft, M.I.; Review & Editing, M.I., S.K, and M.O.; Supervision, S.K, V.P. and M.O.; Funding Acquisition, S.K. All authors have read this revised manuscript and agreed to this contribution list.

References

1. Hobbacher, A. F. *International Institute of Welding-Recommendations for Fatigue Design of International Institute of Welding-Recommendations Welded Joints and Components IIW-1823-07*. *International Institute of Welding* (2008).

2. Corigliano, P. & Crupi, V. Review of Fatigue Assessment Approaches for Welded Marine Joints and Structures. *Metals* vol. 12 (2022).

3. China Classification Society. *Guidelines for Fatigue Strength Assessment of Offshore Engineering Structures-Guidance Note GD 09-2013*. (2013).

4. Potvin, A. B., Kuang, J. G., Leick, R. D. & Kahlich, J. L. Stress Concentration in Tubular Joints. *Soc. Pet. Eng.* 287–299 (1977).

5.   A. C. Wordsworth, G. P. S. Stress Concentration at Unstiffened Tubular Joints. in *European Offshore Steel Research Seminar* (1878).

6.   Wordsworth, A. C. Stress Concentration Factors at K and KT tubular joints. in *Fatigue in Offshore Structural Steels* 59–66 (Thomas Telford Publishing, 1981).

7.   Efthymiou, M. Development of SCF formulae and generalized influence functions for use in fatigue analysis. in *Recent Developments in Tubular Joints Technology (OTJ 88)* (UEG Offshore Research, 1988).

8.   Lloyd's Register. Stress Concentration Factors for Tubular Complex Joints. *Lloyd's Regist. Shipp. Heal. Saf. Exec. - Offshore Technol. Rep. (OTH 91 353)* (1992).

9.   Lloyd's Register. Stress Concentration Factors for Simple Tubular Joints. *Lloyd's Regist. Shipp. Heal. Saf. Exec. Technol. Repor (OTH 354)* (1997).

10.   Diaye, A. N., Hariri, S., Pluvinage, G. & Azari, Z. Stress concentration factor analysis for welded, notched tubular T-joints under combined axial, bending and dynamic loading. *Int. J. Fatigue* **31**, 367–374 (2009).

11.   Gulati, K. C., Wang, W. J. & Kan, D. K. Y. An analytical study of stress concentration effects in multibrace joints under combined loading. in *Offshore Technology Conference* vols 1982-May 337–342 (1982).

12.   API. *Recommended practice for planning, designing and constructing fixed offshore platforms-API RP2A*. (API Publishing Services, 1993).

13.   Ahmadi, H., Lotfollahi-Yaghin, M. A. & Aminfar, M. H. Geometrical effect on SCF distribution in uni-planar tubular DKT-joints under axial loads. *J. Constr. Steel Res.* **67**, 1282–1291 (2011).

14.   Lotfollahi-Yaghin, M. A. & Ahmadi, H. Effect of geometrical parameters on SCF distribution along the weld toe of tubular KT-joints under balanced axial loads. *Int. J. Fatigue* **32**, 703–719 (2010).

15.   Ahmadi, H., Lotfollahi-Yaghin & Mohammad, A. Experimental and Numerical Investigation of Geometric SCFs in Internally Ring-Stiffened Tubular KT-Joints of Offshore Structures. *J. Persian Gulf* **4**, 1–12 (2013).

16.   Zavvar, E., Sadat Hosseini, A. & Lotfollahi-Yaghin, M. A. Stress concentration factors

in steel tubular KT-connections with FRP-Wrapping under bending moments. *Structures* **33**, 4743–4765 (2021).

17. Vijaya Kumar, S. D., Karuppanan, S., Perumal, V. & Ovinis, M. Failure Pressure Prediction of Corroded High-Strength Steel Pipe Elbow Subjected to Combined Loadings Using Artificial Neural Network. *Mathematics* **11**, (2023).

18. Tohidi, S. & Sharifi, Y. Load-carrying capacity of locally corroded steel plate girder ends using artificial neural network. *Thin-Walled Struct.* **100**, 48–61 (2016).

19. Miao, K., Pan, Z., Chen, A., Wei, Y. & Zhang, Y. Machine learning-based model for the ultimate strength of circular concrete-filled fiber-reinforced polymer–steel composite tube columns. *Constr. Build. Mater.* **394**, 132134 (2023).

20. Dabiri, M., Ghafouri, M., Raftar, H. R. R. & Björk, T. Neural network-based assessment of the stress concentration factor in a T-welded joint. *J. Constr. Steel Res.* **128**, 567–578 (2017).

21. Ahmadi, H., Lotfollahi-Yaghin, M. A. & Aminfar, M. H. Effect of stress concentration factors on the structural integrity assessment of multi-planar offshore tubular DKT-joints based on the fracture mechanics fatigue reliability approach. *Ocean Eng.* **38**, 1883–1893 (2011).

22. Zavvar, E., Henneberg, J. & Guedes Soares, C. Stress concentration factors in FRP-reinforced tubular DKT joints under axial loads. *Mar. Struct.* **90**, 103429 (2023).

23. ARSEM (Association de recherche sur les structures métalliques marines). *Welded tubular joints-Design guides for offshore structures*. vol. 1 (Technip, Peris France, 1987).

24. International Standard Organization. *Petroleum and natural gas industries — Fixed steel offshore structures (ISO-19902)*. www.iso.org (2007).

25. Ahmadi, H. & Nejad, A. Z. Stress Concentration Factors in Uniplanar Tubular KT-Joints of Jacket Structures Subjected to In-Plane Bending Loads. *Int. J. Marit. Technol. IJMT* **5**, 27–39 (2016).

26. Ahmadi, H. Probabilistic analysis of the DoB in axially-loaded tubular KT-joints of offshore structures. *Appl. Ocean Res.* **87**, 64–80 (2019).

27. Ahmadi, H. & Zavvar, E. Degree of bending (DoB) in offshore tubular KT-joints under

the axial , in-plane bending (IPB), and out-of-plane bending (OPB) loads. *Appl. Ocean Res.* **95**, 102015 (2020).

28. Hectors, K. & De Waele, W. Influence of weld geometry on stress concentration factor distributions in tubular joints. *J. Constr. Steel Res.* **176**, 106376 (2021).

29. Ahmadi, H. & Lotfollahi-Yaghin, M. A. Stress concentration due to in-plane bending (IPB) loads in ring-stiffened tubular KT-joints of offshore structures: Parametric study and design formulation. *Appl. Ocean Res.* **51**, 54–66 (2015).

30. Ahmadi, H., Yeganeh, A., Mohammadi, A. H. & Zavvar, E. Probabilistic analysis of stress concentration factors in tubular KT-joints reinforced with internal ring stiffeners under in-plane bending loads. *Thin-Walled Struct.* **99**, 58–75 (2016).

31. Ferro, P. & Petrone, N. Asymptotic thermal and residual stress distributions due to transient thermal loads. *Fatigue Fract. Eng. Mater. Struct.* **32**, 936–948 (2009).

32. Ferro, P., Berto, F. & James, N. M. Asymptotic residual stress distribution induced by multipass welding processes. *Int. J. Fatigue* **101**, 421–429 (2017).

33. Iqbal, M., Karuppanan, S., Perumal, V. & Ovinis, M. Rehabilitation Techniques for Offshore Tubular Joints. *J. Mar. Sci. Eng.* **11**, 461 (2023).

34. Bao, S., Wang, W., Li, X., Qi, S. & Zhou, J. Experimental study of hot spot stress for three-planar tubular Y-joint: II. Combined loads. *Thin-Walled Struct.* **177**, 109416 (2022).

35. Hoon, K., Wong, L. & Soh, A. Experimental investigation of a doubler-plate reinforced tubular T-joint subjected to combined loadings. *J. Constr. Steel Res.* **57**, 1015–1039 (2001).

36. Vijaya Kumar, S. D., Lo, M., Karuppanan, S. & Ovinis, M. Empirical Failure Pressure Prediction Equations for Pipelines with Longitudinal Interacting Corrosion Defects Based on Artificial Neural Network. *J. Mar. Sci. Eng.* **10**, (2022).

37. Soh, A.-K. & Soh, C.-K. Stress analysis of axially loaded T tubular joints reinforced with doubler plates. *Comput. Struct.* **55**, 141–149 (1994).

38. Morgan, M. R. & Lee, M. M. K. New parametric equations for stress concentration factors in tubular K-joints under balanced axial loading. *Int. J. Fatigue* **19**, 309–317

(1997).

39.   Pang, H. L. J. & Lee, C. W. Three-dimensional finite element analysis of a tubular T-joint under combined axial and bending loading. *Int. J. Fatigue* **17**, 313–320 (1995).

40.   Yeoh, S. K., Soh, A. K. & Soh, C. K. Behaviour of tubular T-joints subjected to combined loadings. *J. Constr. Steel Res.* **32**, 259–280 (1995).